ISSN 1392–1320 MATERIALS SCIENCE (MEDŽIAGOTYRA). Vol. 19, No. 3. 2013

Aging Effects in Irradiated MgH_2; Connection to Hydrogen Production

Sandra KURKO *, Ljiljana MATOVIĆ, Radojka VUJASIN, Igor MILANOVIĆ, Željka RAŠKOVIĆ-LOVRE, Nenad IVANOVIĆ, Jasmina GRBOVIĆ NOVAKOVIĆ

Vinča Institute of Nuclear Sciences, University of Belgrade, P.O Box 522, 11000 Belgrade, Serbia

crossref http://dx.doi.org/10.5755/j01.ms.19.3.2308

Received 26 August 2012; accepted 06 January 2013

The paper deals with the possibility to control aging of MgH_2 by controlling the deposited energy, number and type of defects and their distribution in the near surface region using Ar^{8+}, Xe^{8+}, and B^{3+} ion irradiation. The evolution of the obtained phases was monitored using X-ray diffraction (XRD), scanning electron microscopy (SEM), Raman spectroscopy, laser scattering particle size distribution measurements and surface area analyses. Obtained results give the possibility to resolve between the material related (impurities, defects, strains) and the ambient induced component of aging.

Keywords: $MgH_2/Mg(OH)_2$ composite, aging, irradiation, deposition of defects.

1. INTRODUCTION

One promising technology for clean, cheap and efficient energy production involves hydrogen storage in metals. Due to its high hydrogen capacity by weight (7.6 wt.%), its abundance in the Earth's crust and its low cost, Mg and its alloys have been extensively studied for this purpose [1–8]. The main obstacles preventing MgH_2 commercial applications are its high stability, which leads to a high desorption temperature, low plateau pressure at ambient temperature [1, 2] and its strong tendency for oxidation and corrosion, which hinders the hydrogen sorption.

Despite the fact that the extensive theoretical [7, 8] and experimental [1–6] work have provided a significant progress in H sorption kinetics, the problem of oxidation is still remaining. It has been demonstrated that not only direct exposure of MgH_2 powder to the air, but also the contamination of inert atmosphere in a glove box can lead to the formation of $MgO/Mg(OH)_2$ layer on MgH_2 particle surface and steadily deteriorate the material performances [9]. Dealing with this problem, it has been established [10–12] that hydrolysis of MgH_2 could be an alternative route for H production due to formation of oxide/hydroxide layer. The $MgO/Mg(OH)_2$ layer formation and decomposition is related to the release of H_2 through following reactions:

$$MgH_2+2H_2O \rightarrow Mg(OH)_2+2H_2 \ (\Delta H = -68 \text{ kJ/mol}H_2), \quad (1)$$

$$MgH_2+Mg(OH)_2 \rightarrow 2MgO+2H_2 \ (\Delta H = -101.7 \text{ kJ/mol}H_2). \quad (2)$$

The large amount of H_2 released, together with the low cost of involved materials makes them worth of consideration for the commercial applications.

In this paper we have investigated the possibility to control aging of MgH_2 samples, using ion irradiation. Using ion irradiation it is possible to govern the deposited energy, number and type of defects and their distribution in exact way, especially in the near surface region. The evolution of obtained phases was monitored using XRD, SEM, Raman, Laser Scattering Particle Size Distribution Measurements and Surface Area Analyses.

2. EXPERIMENTAL DETAILS AND EXPERIMENTAL RESULTS

The samples are prepared and irradiated as it was explained in our previous papers [3–5]. The commercial MgH_2 (Alfa Aeser, 98 %) is denoted as AA, while the samples S16, A16 and B16 are samples irradiated with 120 keV Xe^{+8} and Ar^{+8}, and 45 keV B^{3+} ions, respectively. The used fluence was 10^{16} ion/cm^2 for all investigated samples. After irradiation, the samples were exposed simultaneously to the air for the equal period of time (one moth).

Microstructure of samples was determined using XRD analysis by means of Siemens KRISTALLOFLEX D-500 device with Cu-K_α Ni filtrated radiation (λ = 1.5406 Å). The diffracted X-rays were collected over 2θ range 10°–90° using a step width of 0.02° with measuring time of 1 s per step. The angular correction was done by high quality Si standard. The phase composition, size and strain were calculated using PowderCell 2.4. Particle size distribution and surface area analysis were done using Malvern 2000SM Mastersizer laser scattering particle size analysis system operating in the range from sub-μm to 2 mm in 2-propanol as suspension media. XRD patterns of samples irradiated with the same ion fluence 10^{16} ion/cm^2 of Ar (A16), Xe (S16) and boron ions (B16) are presented in Fig. 1. Morphological and microanalytical characterization was carried out by SEM analyses using VEGA TS 5130MM, Tescan Brno SEM equipped with EDS detector. The results are given on micrographs (Figure 2).

Raman spectra were obtained at Jobin Yvon model T64000 monochromator, with a CCD detector. The spectra are presented in Fig. 3. Raman spectra of all samples show three main maxima at 311, 957 and 1278 cm^{-1} corresponding to Raman active B_{1g}, E_g and A_{1g} MgH_2 phonons respectively. The aged samples exhibit also Raman active vibrations corresponding to brucite ($Mg(OH)_2$) at 257, 275, 280, 445 cm^{-1} [19–24]. MgH_2 bands at 957 cm^{-1} and 1278 cm^{-1} can be assigned to optical phonons, which are dominated by H vibrations, while the band at 311 cm^{-1} corresponds to acoustic phonons

*Corresponding author. Tel.:+381-11-3408507, fax: +381-11-3408224, E-mail address: *skumric@vinca.rs* (S. Kurko)

determined mainly by Mg vibrations [4, 22]. Brucite has trigonal P-3m1 crystal structure with five atoms in the unit cell, Mg atoms being at 1a (0 0 0), and OH group at 2d (1/3 2/3 z) Wyckoff positions, providing 15 normal modes $2A_{1g} + 3A_{2u} + 2E_g + 3E_u$ in the Brillouin-zone (BZ). The acoustic modes are formed of collective A_{2u}, and E_u vibrations. Factor group analysis gives six allowed lattice modes for brucite: three of them are infrared, and three are Raman active [21]. Translational modes correspond to OH vibrations that are either parallel [A_{1g}(T) and A_{2u}(T)], or perpendicular [E_g(T) and E_u(T)] to the c axis. Rotational OH spectra are composed of E_{1g}(R) and E_u(R) modes. The internal OH modes consist of symmetric (Raman active, A_{1g}(I)) and antisymmetric (infrared – active, A_{2u}(I)) O–H stretching vibrations. Raman shift is large for the high frequency modes, which are dominated by the hydrogen motion and small for the low-frequency modes, which involve Mg and rigid translations of the entire OH group. Reynard [23] explained the $Mg(OH)_2$ Eg mode at 257 cm^{-1} involves displacements of OH groups in planes parallel to (001), leading to the shear of the OH octahedra around Mg, in the way that OH groups in alternate planes vibrate in the opposite directions. The A_{1g} mode around 445 cm^{-1} is a breathing mode of the OH octahedra so the OH translation can also take place in the direction perpendicular to the layer. These modes are experimentally detected (Table 2) in the surface layer of our samples after the aging confirming formation of $Mg(OH)_2$ and therefore formation of composite material.

3. DISCUSSION

From the XRD patterns presented in Fig. 1 one can notice that intensity of β-MgH_2 peaks (ICSD:155807 MgH_2) in the aged samples is reduced compared to the non-irradiated [3] and the irradiated samples before aging [3 – 5].

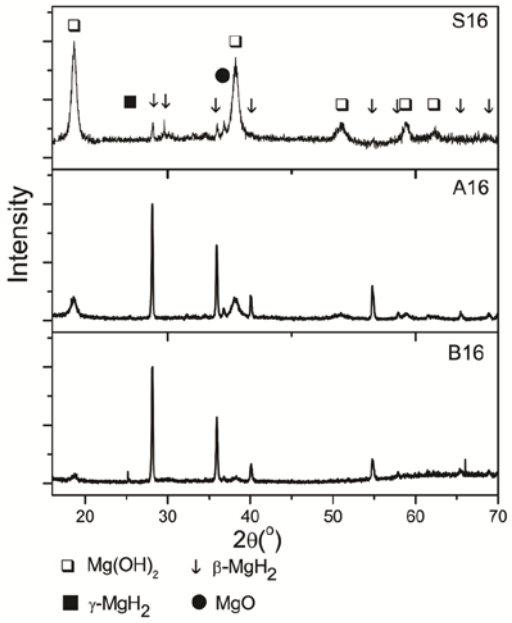

Fig. 1. XRD patterns of MgH_2 powders irradiated with: 120 keV Ar^{8+} (A16), 120 keV Xe^{8+} (S16) and 45 keV B^{3+} ions at fluence of 10^{16} ion/cm^2 after one month aging

Formation of $Mg(OH)_2$ (peaks at 2θ~18º and ~38º, ICSD:165674-$Mg(OH)_2$) due to reaction of MgH_2 with environmental moisture (H_2O) (reaction 1) has been observed in all samples [12 – 17]. Different ratios of hydride and hydroxide phases were formed in various samples, following the initial defect concentration implemented by ion irradiation (see Table 1). The smallest amount of $Mg(OH)_2$ phase is noticed in the aged B16 sample, while noticeable larger one is present in the aged A16 sample. In the S16 sample, quantity of formed $Mg(OH)_2$ is considerably higher than in the other two. Such behavior has been attributed to the fact that Xe is the heaviest of three used ions meaning that, at the same fluence will produce much more defects. Further, those defects are deposited closer to the sample surface (within 80 nm in this case, see Table 1). In this way the highly reactive sub-surface layer was formed enabling the fastest reaction with the moisture. This process did not take place in A16 and B16 samples, where maximum of the defects are placed deeper inside the sample and its concentration is significantly lower [4, 5]. Therefore the critical defects concentration in the sub-surface has to be reached, to enable the faster hydrolysis reaction through all sample volume, meaning that by controlling the depth and quantity of defects we can control the properties of material. The ion irradiation induced also the reduction of particle size, which is the largest for the S16 sample, but comparable for samples A16 and B16. The particle size distribution and specific surface area are obtained using so called "equivalent spherical diameter" meaning that all particles have spherical shape. The obtained specific surface area depends on particle shape, surface irregularities and porosity. Although, the obtained value for the specific surface area of sample irradiated with boron is quite large, the amount of $Mg(OH)_2$ phase formed under the same conditions is considerably smaller than other two samples. This actually gives rise to the conclusion that reduction of particle size and therefore specific surface area depends on the depth deposition of defects, not on the quantity of formed vacancies. Therefore, by controlling the depth deposition of defects one can govern the process of $Mg(OH)_2$ formation i. e. control both reactions (1) and (2). Fig. 2 shows SEM micrographs of irradiated samples after one month of aging. The surfaces of aged samples are very rough due to formation of $Mg(OH)_2$. The onion-like structure [4] which originates from constant cracking in the border region of MgH_2 particles has disappeared. According to Leardini [18] this pronounced surface roughness comes from the increase of material molar volume and the related strains accompanying the hydride to hydroxide transformation (see Table 1). In the A16 and S16 samples dimensions of agglomerates range between 50 μm and 120 μm while in the B16 sample the agglomerates size is between 10 μm and 40 μm.

Raman spectra of the commercial sample after aging and samples irradiated with different ions after aging are presented in Fig. 3. The results summarized in Table 2, together with some experimental and theoretical [19 – 24] data of other authors give clear picture about the changes obtained after irradiation and aging. Raman spectra confermed the masive formation of hydroxide.

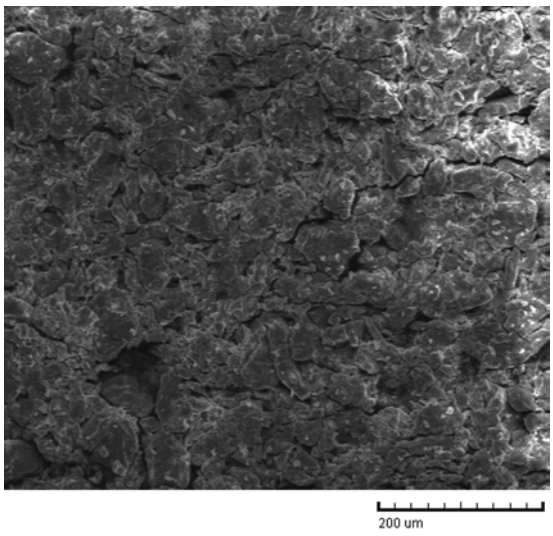

a

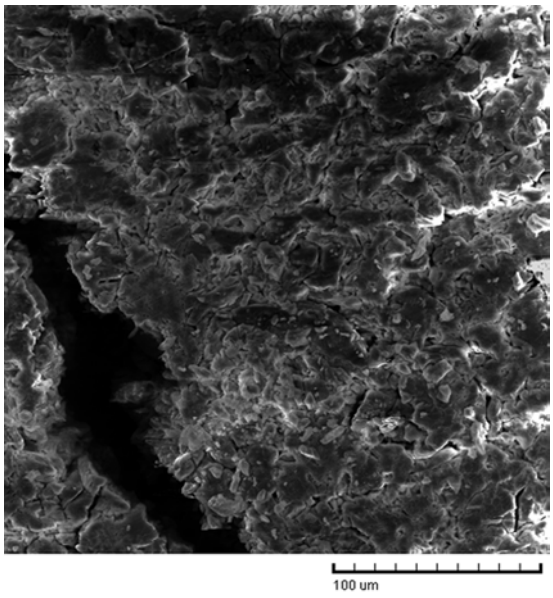

b

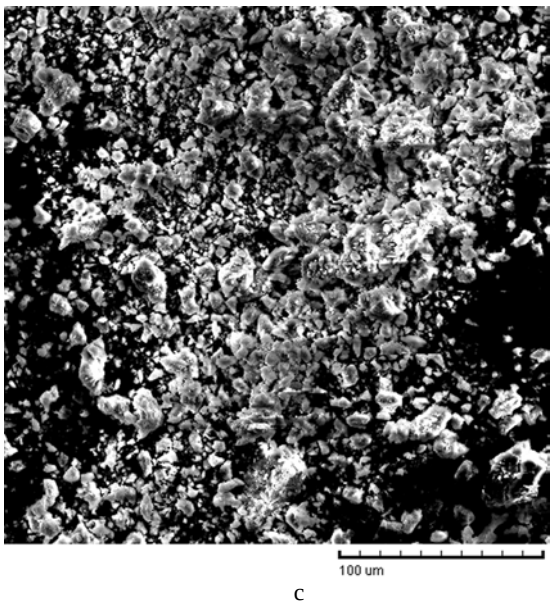

c

Fig. 2. SEM micrographs of irradiated powders with (a) 120 keV Ar^{8+} (A16), (b) 120 keV Xe^{8+} (S16) and (c) 45 keV B^{3+} ions at fluence of 10^{16} ion/cm^2 after one month aging

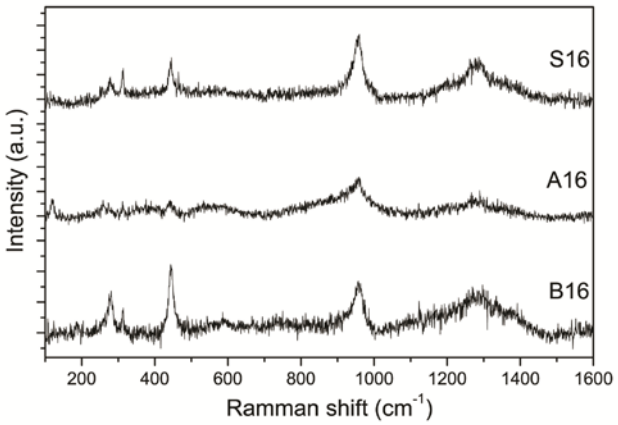

Fig. 3. Raman spectra of samples irradiated with 120 keV Ar^{8+} (A16), 120 keV Xe^{8+} (S16) and 45 keV B^{3+} ions at fluence of 10^{16} ion/cm^2 after one month aging

The recent work of Leardini et al. [18] showed that solid-state reactions at $MgH_2/Mg(OH)_2$ interface give rise to additional hydrogen desorption through two different channels. The first (denoted LT-H_2) arises from the reaction between a H atom coming from MgH_2, and a $Mg(OH)_2$ surface OH group. The second one (IT-H_2) is opened by the reaction between a H atom from MgH_2, and another coming from $Mg(OH)_2$ at the $MgH_2/Mg(OH)_2$ interface. According to the authors, the onset of the MgH_2 desorption process (HT-H_2) is controlled by the incubation time necessary for creation of the catalytically active sites by dehydroxylation of the $MgH_2/Mg(OH)_2$ surface layer. Once these sites are formed, the reaction mechanism changes. The catalytically active sites, presumably vacancies and their complexes, their distribution in the sub-surface region noticeably influence the hydrolysis reaction. Consequently, it is possible to improve significantly the yield and kinetics of hydrolysis reaction by appropriate control of defects acting as hydrolysis reaction activation centers, without catalysts addition.

4. CONCLUSSIONS

Using XRD, SEM, Raman spectroscopy and laser particle size analysis was monitored a formation of hydroxide layer at the surfaces of MgH_2 samples irradiated by 10^{16}/cm^2 heavy ions of Ar^{8+}, Xe^{8+} accelerated at 120 keV, and B^{3+} accelerated at 45 keV. $MgH_2/Mg(OH)_2$ composites with different proportions of hydride and hydroxide phases have been formed in all samples, following various defect concentrations and penetration depth of different ions. In the sample irradiated with Xe^{8+} quantity of formed $Mg(OH)_2$ is considerably higher than in the other two samples, comprising almost entire volume of the sample. This is due to the fact that irradiation with the heaviest of three ions produces for the same fluence much more defects and that these defects are distributed closer to the sample surface. The results suggest that under ambient conditions there is a critical defect (or catalytically active sites) concentration and depth deposition in the MgH_2 surface layer which must be achieved to enable a complete hydrolysis reaction in the bulk of the sample.

Table 1. Vacancy production and depth deposition of defects obtained by SRIM calculations, particle size and specific surface area obtained by laser scattering particle size analysis of MgH_2 sample irradiated with 10^{16} ion/cm^2 of Ar, Xe and B before aging and phase composition of composites $MgH_2/Mg(OH)_2$ obtained from XRD analysis

Sample	Vacancy/ion	Depth deposition	Particle size (μm)	S (m^2/g)	% MgH_2	% $Mg(OH)_2$	% MgO
AA	/	/	38	0.190	100	0	0
B16	218	216	21	0.572	80.78	11.27	7.95
A16	1248	175	23	0.342	59.42	38.64	1.94
S16	1818	85	14	0.810	16.84	82.88	0.28

Table 2. Raman shifts observed in MgH_2 samples irradiated with 10^{16} ion/cm^2 of Ar^{8+} (A16), Xe^{8+} (S16) and B^{3+} (B16) after one month aging together with experimental and theoretical values of MgH_2 and $Mg(OH)_2$ from literature [19, 20 – 24]

Sample/mode	$Mg(OH)_2$ [cm^{-1}]			MgH_2 [cm^{-1}]		
	E_g (T)*	E_g (L)*	A_{1g}(T)*	B_{1g}	E_g	A_{1g}
S16	257, 280		445	311	957	1278
A16	257, 275		443	311	957	1278
B16	275		443	311	957	1278
[23]	268	767	449, 3686 (I)			
[24]	279	720	445, 3673 (I)			
[20]	280	725	443, 3652 (I)			
[22]/Shell model				312	940	1274
[22]/LAPW				289	963	1277
[19]				300	950	1276

*T – transverse optical mode, L – longitudinal optical mode

Acknowledgments

Ministry of Education, Science and Technology of Republic of Serbia financially supports this work under grant III45012.

REFERENCES

1. **Schlapbach, L., Züttel, A.** Hydrogen-storage Materials for Mobile Applications *Nature* 414 2001: pp. 353 – 358.
2. **Sakintuna, B., Lamari-Darkrim, F., Hirscher, M.** Metal Hydride Materials for Solid Hydrogen Storage: A Review *International Journal of Hydrogen Energy* 32 2007: pp. 1121 – 1140. http://dx.doi.org/10.1016/j.ijhydene.2006.11.022
3. **Matović, Lj., Novaković, N., Kurko, S., Šiljegović, M., Matović, B., Kačarević Popović, Z., Romčević, N., Ivanović N., Grbović Novaković, J.** Structural Destabilisation of MgH_2 Obtained by Heavy Ion Irradiation *International Journal of Hydrogen Energy* 34 2009: pp. 7275 – 7282.
4. **Grbović Novaković, J., Matović, L. J., Drvendžija, M., Novaković, N., Rajnović, D., Šiljegovć, M., Kačarević Popović, Z., Milovanović, S., Ivanović, N.** Changes of Hydrogen Storage Properties of MgH_2 Induced by Heavy Ion Irradiation *International Journal of Hydrogen Energy* 33 2008: pp. 1876 – 1879.
5. **Kurko, S., Matović, Lj., Novaković, N., Matović, B., Jovanović, Z., Paskaš Mamula, B., Grbović Novaković, J.** Changes of Hydrogen Storage Properties of MgH_2 Induced by Boron Ion Irradiation *International Journal of Hydrogen Energy* 36 2009: pp. 1184 – 1189.
6. **Montone, A., Grbovic Novakovic, J., Vittori Antisari, M., Bassetti, A., Bonetti, E., Fiorini, A. L., Pasquini, L., Mirenghi, L., Rotolo, P.** Nano-micro MgH_2-Mg_2NiH_4 Composites: Tayloring a Multichannel System with Selected Hydrogen Sorption Properties *International Journal of Hydrogen Energy* 32 2007: pp. 2926 – 2934. http://dx.doi.org/10.1016/j.ijhydene.2006.12.021
7. **Novaković, N., Matović, L. J., Grbović Novaković, J., Manasijević, M., Ivanović, N.** Ab Initio Study of MgH_2 Formation *Materials Science and Engeneering B* 165 2009: pp. 235 – 238.
8. **Park, M. S., Janotti, A., Van de Walle, C. G.** Formation and Migration of Charged Native Defects in MgH_2: First-principles Calculations *Physical Review B: Condensed Matter and Materials Physics* 80 2009: 064102. http://dx.doi.org/10.1103/PhysRevB.80.064102
9. **Varin, R. A., Li, S., Calka, A., Wexler, D.** Formation and Environmental Stability of Nanocrystalline and Amorphous Hydrides in the 2Mg–Fe Mixture Processed by Controlled Reactive Mechanical Alloying (CRMA) *Journal of Alloys and Compounds* 373 2004: pp. 270 – 286. http://dx.doi.org/10.1016/j.jallcom.2003.11.015
10. **Wang, X. L., Haraikawa, N., Suda, S.** A Study of the Surface Composition and Structure of Fluorinated Mg-based Alloys *Journal of Alloys and Compounds* 231 1995: pp. 397 – 402
11. **Nishimiya, N., Wada, T., Matsumoto, A., Tsutsumi, K.** Hydriding–dehydriding Characteristics of Aged Mg-10%Ni

Alloy Hydride and Water Resistance of Sol-gel Encapsulated Composite *Journal of Alloys and Compounds* 311 2000: pp. 207 – 213.

12. **Huot, J., Liang, G., Schulz, R.** Magnesium-based Nanocomposites Chemical Hydrides *Journal of Alloys and Compounds* 353 2003: pp. L12 – L15. http://dx.doi.org/10.1016/S0925-8388(02)01306-3
13. **Chen, C., Splinter, S. J., Do, T., McIntyre, N. S.** Measurement of Oxide Film Growth on Mg and A1 Surfaces over Extended Periods Using XPS *Surface Science* 382 1997: pp. L652 – L657. http://dx.doi.org/10.1016/S0039-6028(97)00054-X
14. **Varin, R. A., Czujko, T., Wronski, Z. S.** Nanomaterials for Solid State Hydrogen Storage. Springer Science+Business Media, New York, 2009.
15. **Grosjean, M. H., Zidoune, M., Roué, L., Huot, J. Y.** Hydrogen Production via Hydrolysis Reaction from Ball-milled Mg-based Materials *International Journal of Hydrogen Energy* 31 2006: pp. 109 – 119.
16. **Varin, R. A., Li, S., Calka, A.** Environmental Degradation by Hydrolysis of Nanostructured β-MgH_2 Hydride Synthesized by Controlled Reactive Mechanical Milling *Journal of Alloys and Compounds* 376 2004: pp. 222 – 231.
17. **Friedrichs, O., Sánchez-López, J. C., López-Cartés, C., Dornheim, M., Klassen, T., Bormann, R., Fernández, A.** Chemical and Microstructural Study of the Oxygen Passivation Behaviour of Nanocrystalline Mg and MgH_2 *Applied Surface Science* 252 2006: pp. 2334 – 2345. http://dx.doi.org/10.1016/j.apsusc.2005.04.018
18. **Leardini, F., Ares, J. R., Bodega, J., Fernandez, J. F., Ferrer, I. J., Sanchez, C.** Reaction Pathways for Hydrogen Desorption from Magnesium Hydride/Hydroxide Composites: Bulk and Interface Effects *Physical Chemistry Chemical Physics* , 12 2010: pp. 572 – 577. http://dx.doi.org/10.1039/b912964b
19. **Santisteban, J. R., Cuello, G. J., Dawidowski, J., Fainstein, A., Peretti, H. A., Ivanov, A., Bermejo, F. J.** Vibrational Spectrum of Magnesium Hydride *Physical Review B* 62 2000: pp. 37 – 40.
20. **Dawson, P., Hadfield, C. D., Wilikinson, G. R.** The Polarized Infrared and Raman Spectra of $Mg(OH)_2$ and $Ca(OH)_2$ *Journal of Physics and Chemistry of Solids* 34 1973: pp. 1217 – 1225. http://dx.doi.org/10.1016/S0022-3697(73)80212-4
21. **Duffy, T., Meade, C., Fei, Y., Mao, H. K., Hemley, R. J.** High-pressure Phase Transition in Brucite, $Mg(OH)_2$ *American Mineralogist* 80 1995: pp. 222 – 230.
22. **Lasave, J., Dominguez, F., Koval, S., Stachiotti, M. G., Migoni, R. L.** Shell-model Description of Lattice Dynamical Properties of MgH_2 *Journal of Physics of Condensed Matter* 17 2005: pp. 7133 – 7141. http://dx.doi.org/10.1088/0953-8984/17/44/006
23. **Reynard, B., Caracas, R.** D/H Isotopic Fractionation between Brucite $Mg(OH)_2$ and Water from First-principles Vibrational Modelling *Chemical Geology* 262 2009: pp. 159 – 168.
24. **Hase, Y.** Computational Study of the Solid-state Vibrations and Force Field of Magnesium and Calcium Hydroxides *Journal of Brazilian Chemical Society* 17 2006: pp. 741 – 745.